Flexible and Printed Electronics

PAPER • **OPEN ACCESS**

Photocurrent study of all-printed photodetectors on paper made of different transition metal dichalcogenide nanosheets

Flexible and Printed Electronics

OPEN ACCESS

RECEIVED
18 May 2018

REVISED
13 August 2018

ACCEPTED FOR PUBLICATION
29 August 2018

PUBLISHED
27 September 2018

PAPER

Photocurrent study of all-printed photodetectors on paper made of different transition metal dichalcogenide nanosheets

D McManus[1], A Dal Santo[1,2], P B Selvasundaram[3,4], R Krupke[3,4], A LiBassi[2] and C Casiraghi[1]

[1] School of Chemistry, University of Manchester, United Kingdom
[2] Department of Energy, Politecnico di Milano, Italy
[3] Institute of Nanotechnology, Karlsruhe Institute of Technology, D-76021 Karlsruhe, Germany
[4] Institute of Materials Science, Technische Universität Darmstadt, D-64287 Darmstadt, Germany

E-mail: cinzia.casiraghi@manchester.ac.uk

Keywords: 2D materials, inkjet printing, photodetectors

Supplementary material for this article is available online

Abstract

We have inkjet-printed in-plane 'metal–semiconductor–metal' type photodetectors on paper, one of the cheapest flexible substrates, which is also recyclable and foldable, in contrast to traditional plastic substrates. The photodetectors are made by using graphene as electrodes and various transition metal dichalcogenides (TMDs) as photoactive component. In particular, we have tested MoS_2, WS_2, $MoSe_2$ and $MoTe_2$. Large differences in responsivity and sensitivity were observed for all of the TMDs measured, with MoS_2 showing the highest sensitivity and $MoTe_2$ producing the largest response. However, photodetectors made of $MoTe_2$ show a large decrease in responsivity after one week of exposure to air. The wavelength dependence of the responsivity in MoS_2 based devices was further analyzed using a supercontinuum photocurrent spectroscopy setup, with the results suggesting a bolometric or photoelectric origin of the signal. We also report some simple approaches to enhance the device performance and tune the energy range at which the maximum in responsivity or sensitivity is observed.

Introduction

Two-dimensional (2D) materials [1] show unique optical, electronic, and mechanical properties that make them exciting prospects for several applications [2, 3], in particular in opto-electronics [2–4]. Graphene's transparency, conductivity, atomic thickness and strength make it an ideal material for the fabrication of transparent and flexible electrodes [2, 3]. Transition metal dichalcogenides (TMDs) have the empirical formula MX_2; where M is a group 6 transition metal (usually Mo or W) and X is a group 16 calcogen (S, Se or Te). In bulk form, TMDs are layered compounds with an indirect band gap, which changes to direct, upon exfoliating to single layer [5, 6]. Because of their complementary electronic properties, TMDs can be used in combination with graphene to fabricate photodetectors [7]. In particular, the use of solution-processed 2D materials [8–10] is very attractive, due to the ability to cost-effectively produce 2D materials and fabricate devices in a scalable manner on a range of substrates at room temperature.

Amongst all fabrication methods, inkjet printing has been demonstrated to be scalable, versatile and cost-effective for the production of devices on a range of substrates [11–15]. Inkjet-printable inks made by liquid-phase exfoliation (LPE) [8, 16] have been produced in a range of solvents, with the most commonly used being cyclohexanone/terpineol [17, 18] and N-methyl-2-pyrrolidone (NMP) [12–14, 19]. Water-based inkjet-printable inks have also been formulated, reducing toxicity and environmental concerns associated with many organic solvents [11]. The flexibility of LPE has resulted in conducting (e.g. graphene), semiconducting (e.g. TMDs) and insulating (e.g. h-BN) 2D nanosheets inks all being produced, allowing for the production of printed devices solely made of 2D materials. Examples include in-plane [13] and vertically stacked photodetectors [11], read-only memories [11], thin-film transistors [19] and

capacitors [12], although some of those devices have been fabricated with a combination of printing technologies (e.g. spray coating of a one layer and inkjet printing of another material). Despite those works, the characterization of in-plane photodetectors, made from solution-processed 2D materials, is still limited [13, 20]. In [13] the device was fabricated by inkjet printing, but only MoS_2 was studied. The device channels were also very large (~1 mm), which possibly explains the need to use large voltages (up to 40 V). In [20], the channel was 50 μm and several TMDs were studied. However, the devices were not printed, but made by the Langmuir–Blodgett method, which is likely to give films morphology different from that obtained by inkjet printing. Furthermore, in [20] only large and thick flakes (μm sized nanoplatelets) were selected, which are too large to be inkjet printed. Finally, the contacts were made of gold, which may result in a higher Schottky barrier than those observed with graphene contacts, due to Fermi level pinning [21]. The formation of a van der Waals gap between 2D materials and gold contacts can also result in the formation of a tunneling barrier which can be avoided with the use of graphene contacts [21]. Based on these observations, in this work we present a systematic photocurrent study on all inkjet-printed in-plane photodetectors using water-based graphene and TMD inks. In particular, WS_2, MoS_2, $MoSe_2$ and $MoTe_2$ are used as the photoactive element, with the aim of investigating how different TMDs can affect the device performance. The electrodes were made of solution-processed graphene, which has been demonstrated to provide enough high conductivity to be used as electrode in printed devices [11–14, 17–19]. We use two parameters for assessing the suitability of each of the TMDs for use in printed photodetectors: the sensitivity and responsivity. Responsivity (R) is defined as the amount of photocurrent (I_{PC}), with respect to dark conditions, produced per watt (P) of illumination ($R = I_{PC}/P$). The sensitivity ($\sigma_{L/D}$) is given by the ratio of conductivity, measured from the slope of the I–V curve close to the origin, under illumination to dark conductivity ($\sigma_{L/D} = \sigma_{light}/\sigma_{dark}$) [20, 22]. Although it is important when fabricating photodetectors to achieve high responsivity in order to maximize the signal generated, the sensitivity of the photodetector is also important for obtaining a high signal to noise ratio, when detecting small changes in light intensity [20, 23]. The device was directly printed on paper (see Methods), being a cheap, recyclable and foldable substrate. Paper-based electronics is indeed attracting strong interest in the flexible and printed electronics community [24, 25]. For example a photodetector on paper made with organic materials have been recently reported [26]. Although the device was not fully printed, this seminal work shows the importance of fabricating photodetectors with simple techniques directly on paper.

Our results indicate that $MoTe_2$ is the TMD with highest responsivity, but it is also the material with the lowest photosensitivity. In addition, $MoTe_2$ based devices are found to be unstable in air: the responsivity quickly drops down after a day or so, in contrast to devices made with other TMD inks, who are stable for months. Overall, the TMD with the highest sensitivity is MoS_2, in agreement with the results reported in [20], despite the use of a different device fabrication method, formulation and flakes composition. Therefore, the responsivity of this device was further analyzed by using a supercontinuum photocurrent spectroscopy setup. The results suggest a bolometric or photoelectric effect with no photocurrent generated below the band gap of the material. Finally, we demonstrate that it is possible to tune the device responsivity by using gold nanoparticles (AuNPs) or blends of 2D materials in the active channel.

Methods

The following bulk materials were used to prepare the inks: graphite (Aldrich Chemistry, graphite, powder, <45 μm, purity: 99.99%), MoS_2 (Aldrich Chemistry, molybdenum (IV) sulfide, powder, <2 μm, purity: 99%), WS_2 (Aldrich Chemistry, tungsten (IV) sulfide, powder, <2 μm, purity: 99%), $MoSe_2$ (Materion Advanced Materials, molybdenum selenide, ~325 mesh, purity: 99.9%) or $MoTe_2$ (Materion Advanced Materials, molybdenum telluride, crystal size > 10 μm, purity: 99.9%). The powders were dispersed in 100 ml of water-based solvent with a concentration of 3 mg ml^{-1} with 1 mg ml^{-1} of PS1 (Sigma, 1-pyrenesulfonic acid sodium salt, purity > 97.0%) and placed in a bath sonicator (Hilsonic HS 1900, Hilsonic FMG 600) at the constant temperature of 20 °C for 92 h. The obtained dispersions were centrifuged three times with a Sigma 1-14K (Sigma 3-18KS) centrifuge to select a proper monolayer percentage and flake-size in the platelets.

Ink concentration was assessed with UV–vis–NIR spectroscopy, performed with a Varian Cary 5000 spectrophotometer, using the extinction coefficients reported in table S1 of the supplementary material (available online at stacks.iop.org/FPE/3/034005/mmedia) and the Beer–Lambert law. The inks were diluted to 0.5 mg ml^{-1} for printing.

Photodetectors were printed with a Fujifilm Dimatix DMP-2800 piezoelectric inkjet printer. Cartridges with a nozzle diameter of 21 μm were used. Neither the nozzles nor the substrate were heated. Thirty print passes were used for both the photoactive layer and the electrodes. The device was printed on a technical paper (PEL P60) sourced from Printed Electronics Ltd. This substrate ensures optimal printability and good mechanical properties, as compared to untreated paper.

Photoelectrical characteristics of the printed devices were acquired using a Renishaw spectrophotometer to

focus the laser (5× magnification) onto the device while sweeping the voltage and recording the current with a Keithley Sourcemeter 2614 B. The voltage was swept between −5 and 5 V dividing the interval in 3500 steps and averaging the results for 100 μs for each of those. Photocurrent mapping was carried out using a WITec alpha 300 R to focus the laser on the sample (10× magnification). The current was measured while keeping the voltage constant at 20 V with a Keithley Sourcemeter 2614 B, while scanning the laser spot across the device in steps of 1 μm by recording the photocurrent as a function of laser position.

The photocurrent spectrum was acquired using a SuperK Extreme EXW-6 broadband supercontinuum light source (NKT Photonics) with a pulse width of 6 ps at 80 MHz repetition rate. The source was fiber-coupled to a SuperK Select acousto-optic tuneable filter (NKT Photonics) with a filtering unit for the visible spectrum ranging from 500 to 825 nm. The quasi-monochromatic light (∼5 nm FWHM) was coupled via a reflective collimator into a Zeiss Axiotech optical microscope. The sample was directly illuminated with the collimated beam of 2 mm diameter without any objective. The spectral power density was measured with a calibrated photodetector (Ophir PD300R). In order to increase the signal to noise ratio of the photocurrent measurement, the incident light was modulated via the AOTF at 1.213 kHz and the resulting photocurrent was converted to a voltage signal by a DLPCA-200 preamplifier (Femto) and measured using a SR-830 Lock-in Amplifier (Stanford Research Systems) at 300 ms integration time. The source-drain voltage was swept between −5 V and 5 V with a step size of 0.1 V using the auxiliary output of the Lock-in Amplifier. Photocurrent spectra were measured with a step size of 5 nm and the responsivity was calculated by normalizing the photocurrent spectrum with the spectral power density of the collimated beam. All measurements were controlled by proprietary software.

The AuNP coating was prepared by drop-casting a diluted solution of already prepared AuNPs (Sigma Aldrich, AuNPs, 5 nm diameter, OD1, stabilized suspension in 0.1 mM phosphate-buffered saline, reactant free) onto a MoS_2 photodetector and dried under vacuum at room temperature.

Results

2D nanosheet inks were formulated by exfoliating the bulk layered material using sonication-assisted LPE in a water-based inkjet-printable solvent [11]. In detail, 30 mg of graphite flakes (Graphexel, 99.5% grade) and 10 mg of 1-pyrenesulfonic acid sodium salt (PS1, from Sigma Aldrich) were mixed into 10 ml of de-ionized water. The mixture was then sonicated at 300 W using a Hilsonic bath sonicator for 3 days. Afterwards, unexfoliated graphite was removed by centrifugation (Sigma 1-14k refrigerated centrifuge) at 3500 rpm (903 g) for 20 min. The supernatant containing graphene and PS1 in water was collected and then centrifuged again at 15 000 rpm for 1 h to collect the sediment. After centrifugation, the supernatant containing excess amount of PS1 in water was discarded. The precipitate was re-dispersed in the printable solvent [11]. The same process is used for the TMDs. Detailed characterization of the nanosheets is shown in the supplementary information.

The fabricated photodetectors consisted of two interdigitated electrodes printed using graphene, with a TMD printed in between, to act as photoactive element. The device geometry was similar to those demonstrated in [13] using NMP-based inks, albeit with a smaller electrode spacing of ∼50 μm. Note that a 50 μm electrode spacing is used due to the printer having a repeatable deposition resolution of ±25 μm, however a MoS_2 photodetector with an electrode spacing of 25 μm was also produced and showed a significant improvement in sensitivity, when compared with those produced with 50 μm spacing (figure S7). We remark that in this work we aim at studying different photoactive materials, while keeping the geometry of the device fixed, in order to investigate any effect due to the composition and chemistry of the photoactive material. Careful optimization of the device architecture, for a fixed photoactive element, will ensure improvements in responsivity. Figure 1(a) shows the simulated electrode design with a drop diameter of ∼50 μm and figure 1(b) shows an optical image of the complete device.

In order to ensure that the photocurrent was being generated by the TMD, rather than by the printed graphene, a photocurrent map (figure 1(d)) was measured for a MoS_2 based photodetector by scanning a 514.5 nm laser over the red dashed area in figure 1(c). The photocurrent map demonstrates that current is only generated when the laser is scanned over the TMD (white dashed area, figure 1(d)), producing no current when illuminating the area corresponding to the printed graphene. After confirmation that the photocurrent was being produced by the TMD, three additional TMDs were tested as photoactive materials: WS_2, $MoSe_2$ and $MoTe_2$. However, devices fabricated using $MoTe_2$ showed poor stability under ambient conditions and became less conductive (figure S6) in just a few days. This may be due to oxidation or the formation of conductive, distorted octahedral (1T′) nanosheets in addition to semiconducting hexagonal (2H) $MoTe_2$ nanosheets during either the exfoliation process or as a result of applying a bias voltage [27–29]. A similar phase transition from 1T′ to 2H has been observed in the literature [28–30], but further studies are required to investigate the poor air stability observed in these devices. It should be noted that all results presented here for $MoTe_2$ devices have been gathered immediately after printing (<24 h), but it is clear that encapsulation or printing under controlled

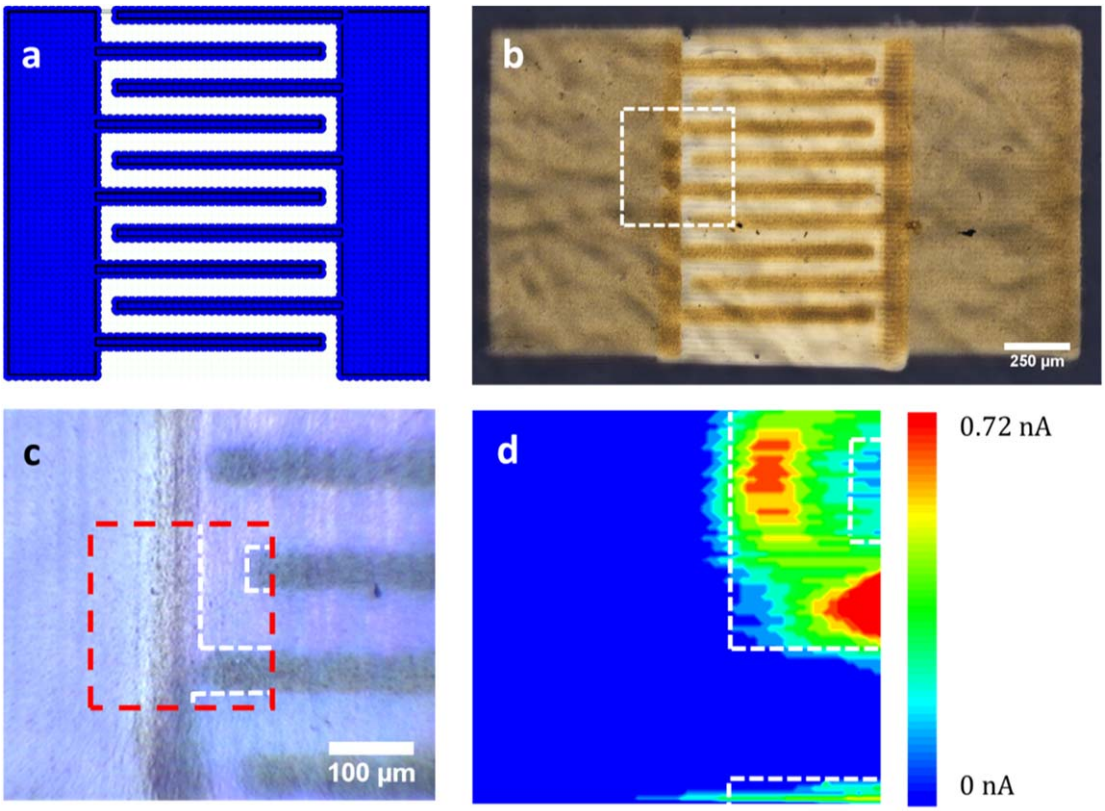

Figure 1. (a) Simulated pattern design of the graphene electrodes showing drop positions on the substrate with drop diameter of ~50 μm. (b) Optical image of the device printed onto PEL P60 paper. (c) Optical image of device corresponding to the dotted white square in panel (b); photocurrent mapping has been measured in the red dotted square. The white dashed lines highlight the boundary of the graphene electrodes. (d) Photocurrent map measured in the red dashed area indicated in (c) with $V_b = 20$ V, $\lambda = 514.5$ nm and $P = 0.5$ mW.

atmosphere may be needed for fabrication of $MoTe_2$ based devices.

The *I–V* characteristics of the MoS_2 photodetector are shown in figure 2(a) for dark conditions and with increasing illumination intensity. The *I–V* curves are symmetric with respect to the origin, with non-Ohmic behavior observed in dark conditions and the *I–V* relationship becoming more linear with increasing laser power. The printed photodetectors show electrical characteristics similar to those produced by Cunningham *et al* [20] and those printed in vertical configurations [11].

Figure 2(b) shows the responsivity across the spectral range for each of the four TMDs measured. $MoTe_2$ gives the highest responsivity, followed by $MoSe_2$. Both MoS_2 and WS_2 give similar values of responsivity across the spectral range. However, the responsivity of $MoTe_2$ photodetectors decreased significantly after one week of atmospheric exposure to below that of both MoS_2 and WS_2. Although $MoTe_2$ shows the highest responsivity across the spectral range (figure 2(b)), the high dark current measured gives rise to low sensitivity at all wavelengths (figure 2(d)). $MoSe_2$ photodetectors showed the second highest responsivity across the spectral range measured, however the high dark current of $MoSe_2$ results in sensitivity similar to those obtained for $MoTe_2$. Despite having the lowest responsivity, MoS_2 photodetectors gave the highest sensitivity across spectral range measured, with 1.69 being the highest value recorded, which was obtained at 488 nm. WS_2 gave the second best sensitivity, with a maximum value of 1.19 at 514.5 nm. We can now compare our results with those reported in [20], where the sensitivity was measured at a fixed wavelength (514 nm): the same trend in sensitivity is observed (figures 2(c) and (d)), despite the different device fabrication method and ink used. However, the values of responsivity and sensitivity are lower compared to those reported in [20]. This may be due to a number of factors, including the increased roughness of paper as a substrate compared to SiO_2, and the reduced conductivity of graphene contacts used in this work compared to the gold contacts used in [20]. As the same trend in sensitivity is observed for photodetectors fabricated using TMDs exfoliated in NMP using gold contacts and TMDs exfoliated in water using graphene contacts, the Fermi level pinning is likely to be produced by the formation of edge defects during the LPE process.

We would now like to discuss the origin of the photoresponse in MoS_2 photodetectors. We have measured in more detail the wavelength dependence of the responsivity using a supercontinuum photocurrent spectroscopy setup employing a lock-in

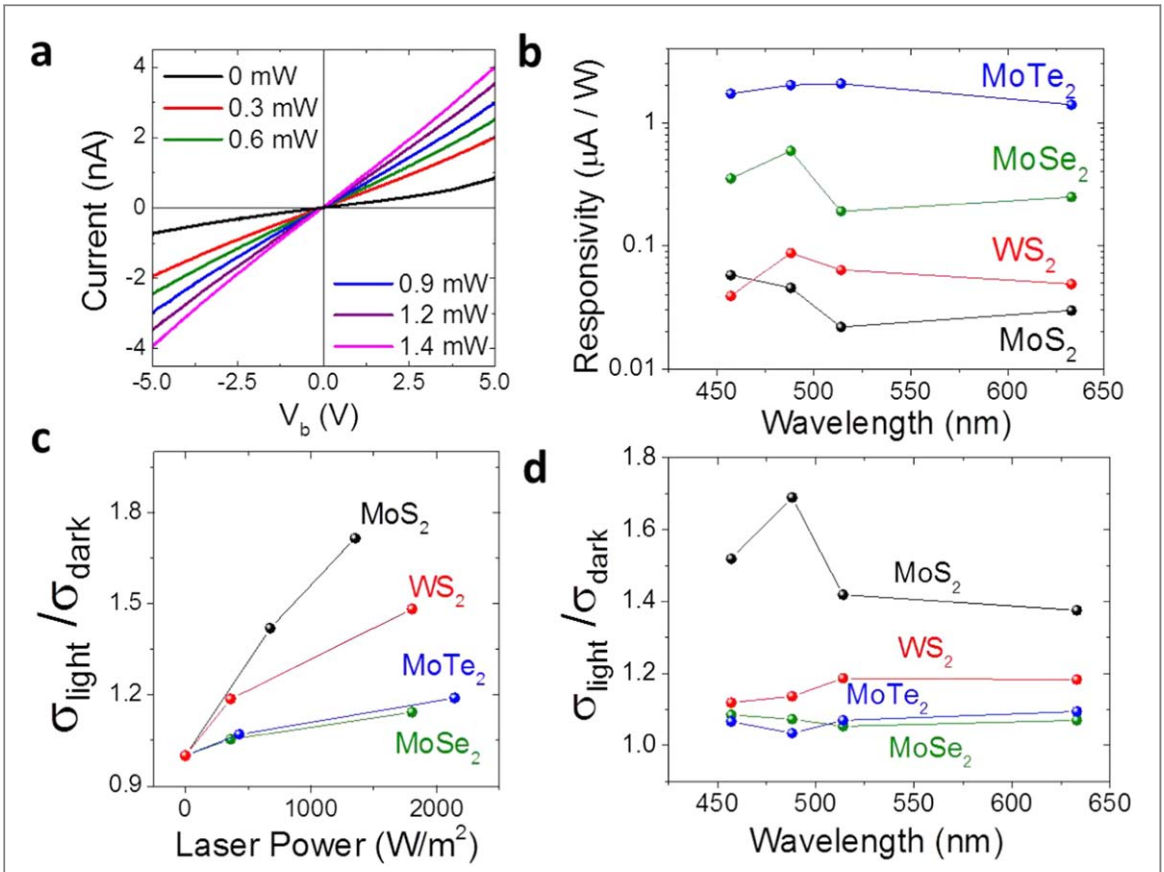

Figure 2. (a) I–V_b plot of a MoS_2 photodetector with 25 μm electrode spacing undergoing illumination with increasing laser power at 488 nm. (b) Responsivity as a function of wavelength for MoS_2, WS_2, $MoSe_2$ and $MoTe_2$ with illumination power <800 mW m^{-2} ($V_b = 1$ V). (c) $\sigma_{L/D}$ ratios plotted as function of laser power for MoS_2, WS_2, $MoSe_2$ and $MoTe_2$ ($\lambda = 514$ nm, $V_b = 1$ V). (d) $\sigma_{L/D}$ ratio as a function of wavelength for MoS_2, WS_2, $MoSe_2$ and $MoTe_2$ with illumination power <800 mW m^{-2} ($V_b = 1$ V).

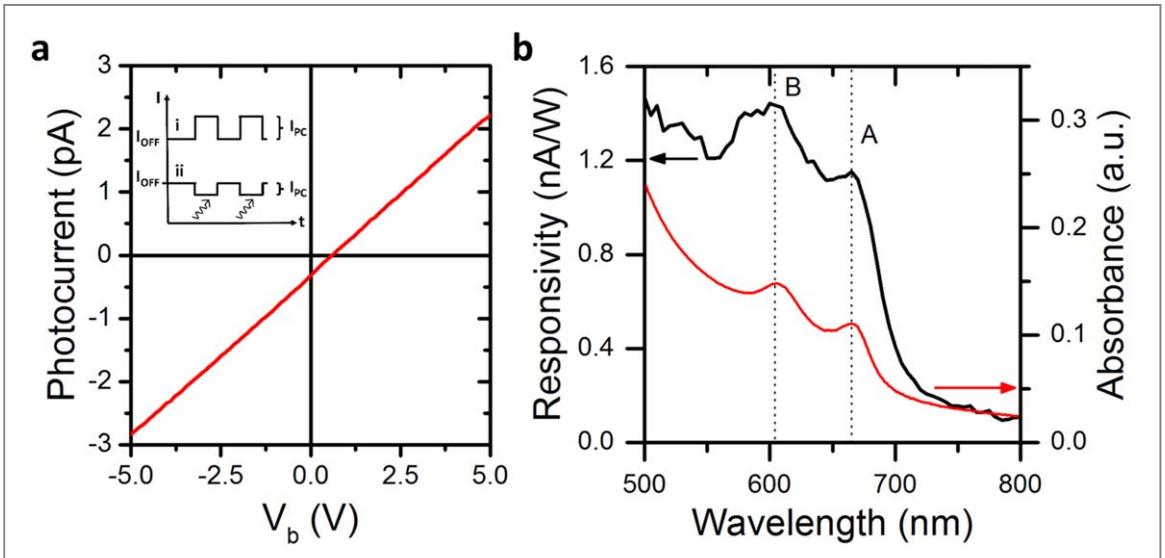

Figure 3. (a) Photocurrent versus bias voltage of a MoS_2 photodetector. Excitation at 665 nm and 1 mW power. The inset illustrates the measurement scheme. (b) Responsivity as a function of wavelength (black line) for MoS_2 at 4 V bias in comparison with the absorption spectrum (red line) of a MoS_2 thin film of similar thickness. The dotted vertical lines mark the energetic positions of the A and B excitons at 665 nm and 606 nm, respectively.

technique. The detected photocurrent signal that we obtain is the difference between the current with and without illumination (inset figure 3(a)). In principle the sign of the photocurrent I_{PC} can be positive or negative as illustrated in (i) and (ii) in the inset of figure 3(a), respectively, and it depends on the light conversion mechanism [31]. The photocurrent versus bias voltage of MoS_2, measured at 665 nm is shown in figure 3(a). It is positive and increases during illumination. The origin of the photoconductivity could be

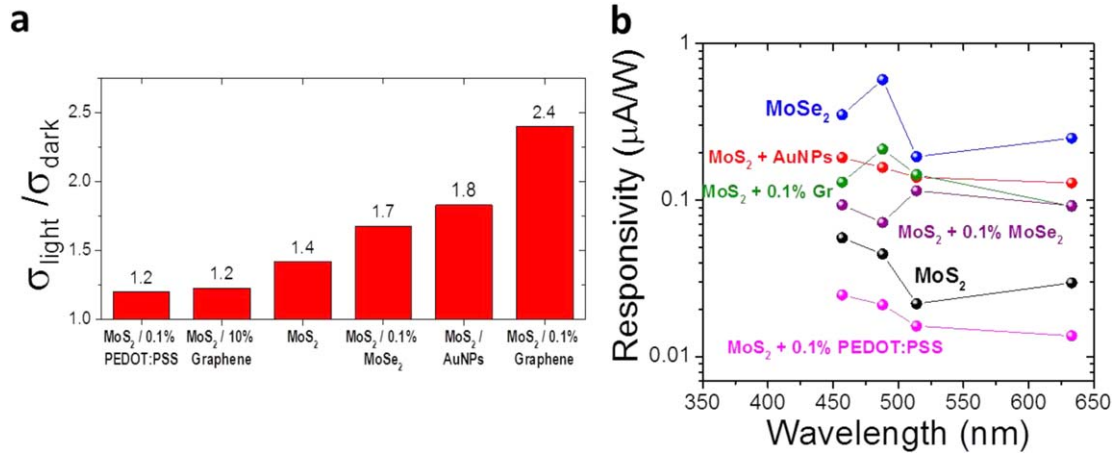

Figure 4. (a) $\sigma_{L/D}$ ratios for a MoS_2, $MoSe_2$ and various modified MoS_2 photodetectors measured at 514.5 nm ($P < 800$ W m^{-2}, $V_b = 1$ V). (b) Responsivity for MoS_2, $MoSe_2$ and various modified MoS_2 photodetectors as a function of the laser wavelength ($P < 800$ W m^{-2}, $V_b = 1$ V).

thermal- or photo-excitation of carriers, typical for a semiconducting material. The responsivity spectrum of MoS_2 in figure 3(b) shows a close correlation to the absorption spectrum measured on a film of similar thickness. The absorption peaks in the absorption spectrum, which have their origin in the generation of A and B excitons due to direct transitions at the K point of the Brillouin zone, appear as peaks in the responsivity spectrum. Compared to absorption measurements on exfoliated MoS_2 with defined number of layers, as in [32], the peaks in the absorption and responsivity spectra appear rather broad. This is however expected, since the exciton transition energy scales inversely with the number of layers, and we have measured in this work inkjet-printed films with a distribution of flake thicknesses (supplementary information). The close correlation between photocurrent and the absorption spectrum energy dependence suggest a bolometric or photoelectric origin of the signal [7], as also confirmed by the absence of signal below the band gap of the material. We remark however that measurements on more efficient devices need to be performed to fully confirm this observation. Note that despite the small responsivity, the devices show stable photocurrent generated under pulsed photoexcitation (figure S9).

In order to improve the photoresponse of the printed devices, a number of photodetectors containing blends of MoS_2 with other 2D materials were fabricated. The first of such blended devices contained between 0.1% and 10% by weight graphene: the addition of graphene should improve the transport of the photoactive layer. However, increasing the graphene content towards the percolation threshold is disadvantageous as it will lead to large increases in dark current [33]. Devices produced with 0.1% graphene by weight had significant sensitivity and responsivity increases when compared with devices containing only MoS_2 (figure 4). At 514 nm, the sensitivity increased from 1.4 for MoS_2, to 2.4 for the MoS_2/0.1% graphene blend (figure 4(a)). The responsivity increased by around one order of magnitude across the wavelengths measured. When the graphene loading was increased further, the sensitivity and responsivity decreased below the values found for MoS_2 (figure 4(a)).

A similar strategy for increasing the sensitivity and responsivity was attempted by blending MoS_2 with 0.1% poly 3,4-ethylenedioxithiophene polystyrene sulfonate (PEDOT:PSS). All devices showed poorer performance when compared with MoS_2 without any polymer (figure 4). The reduced sensitivity for 0.1% PEDOT:PSS may be a result of the percolation threshold being reached with a lower weight percentage loading, due to the large difference in the aspect ratios of PEDOT:PSS and graphene.

A blend of two TMDs was then used to increase the responsivity and sensitivity. MoS_2 was blended with 0.1 and 1 weight percent $MoSe_2$. $MoSe_2$ was chosen due to the higher value of σ_{dark} compared to MoS_2 and the alignment of the conduction band with that of MoS_2 [34, 35]. Devices fabricated using 0.1% $MoSe_2$ showed an improvement in the sensitivity from 1.4 to 1.7 at 514 nm and increased responsivity across the measured range (figure 4). As the $MoSe_2$ percentage was increased to 1%, the sensitivity lowered to below that of pure MoS_2.

Finally, we investigated a third approach based on the use of plasmonic nanostructures, which have been demonstrated to increase the responsivity of TMD-based photodetectors fabricated by mechanically-exfoliation [36]. Drop-casting AuNPs onto a MoS_2 photodetector led to a shift in the wavelengths at which maximum responsivity and sensitivity were observed (figure 4). In figure 4(a), a large increase in photosensitivity and responsivity is observed at 514 nm due to plasmonic resonance of the AuNPs (figure S8). The photosensitivity increases from 1.4 to 8.3 (figure 4(a)) at 514 nm due to the dark conductivity

remaining the same as for uncoated MoS_2, while the light conductivity increases significantly, as can be observed from the increase in responsivity.

Conclusions

Herein, we have shown an extensive investigation on all inkjet-printed, 2D-material photodetectors on paper, using a variety of TMDs. The results for photosensitivity obtained show good agreement with similar devices fabricated using flakes obtained by LPE in NMP [20], demonstrating that water-based inks can also be used to make such devices and that their performance strongly depends on the nature of the photoactive material used. As the TMDs demonstrated similar photoelectrical characteristics with both gold [20] and graphene contacts, further work is required to make more efficient contacts to avoid Fermi level pinning. A number of methods for increasing photosensitivity were investigated, enabling increases in performance to be achieved through the addition of plasmonic nanostructures or blending of various 2D materials. As blending of a small amount of graphene into the TMD was shown to be an efficient strategy for improving device performance, it may prove useful for improving other devices utilizing LPE TMDs, such as printed transistors [19]. In particular, the approaches of using graphene or $MoSe_2$ blends and coating MoS_2 photodetectors with AuNPs provided the dual benefits of increasing both the photodetector sensitivity and responsivity.

Acknowledgments

This work is partially supported by the EPSRC in the framework of the CDT Graphene Nownano and Grand Challenge grant EP/N010345/1.

ORCID iDs

D McManus https://orcid.org/0000-0002-8494-0870
C Casiraghi https://orcid.org/0000-0001-7185-0377

References

[1] Novoselov K S *et al* 2005 Two-dimensional atomic crystals *Proc. Natl Acad. Sci.* **102** 10451–3
[2] Ferrari A C *et al* 2015 Science and technology roadmap for graphene, related two-dimensional crystals, and hybrid systems *Nanoscale* **7** 4598–810
[3] Novoselov K S *et al* 2012 A roadmap for graphene *Nature* **490** 192–200
[4] Mak K F and Shan J 2016 Photonics and optoelectronics of 2D semiconductor transition metal dichalcogenides *Nat. Photon.* **10** 216–26
[5] Mak K F, Lee C, Hone J, Shan J and Heinz T F 2010 Atomically thin MoS_2: a new direct-gap semiconductor *Phys. Rev. Lett.* **105** 136805
[6] Splendiani A *et al* 2010 Emerging photoluminescence in monolayer MoS_2 *Nano Lett.* **10** 1271–5
[7] Koppens F H *et al* 2014 Photodetectors based on graphene, other two-dimensional materials and hybrid systems *Nat. Nanotechnol.* **9** 780–93
[8] Hernandez Y *et al* 2008 High-yield production of graphene by liquid-phase exfoliation of graphite *Nat. Nanotechnol.* **3** 563–8
[9] Paton K R *et al* 2014 Scalable production of large quantities of defect-free few-layer graphene by shear exfoliation in liquids *Nat. Mater.* **13** 624–30
[10] Coleman J N *et al* 2011 Two-dimensional nano-sheets produced by liquid exfoliation of layered materials *Science* **331** 568–71
[11] McManus D *et al* 2017 Water-based and biocompatible 2D crystal inks for all-inkjet-printed heterostructures *Nat. Nanotechnol.* **12** 1–19
[12] Kelly A G, Finn D, Harvey A, Hallam T and Coleman J N 2016 All-printed capacitors from graphene-BN-graphene nanosheet heterostructures *Appl. Phys. Lett.* **109** 23107
[13] Finn D J *et al* 2014 Inkjet deposition of liquid-exfoliated graphene and MoS_2 nanosheets for printed device applications *J. Mater. Chem.* C **2** 925–32
[14] Torrisi F *et al* 2012 Inkjet-printed graphene electronics *ACS Nano* **6** 2992–3006
[15] Hu G *et al* 2017 Black phosphorus ink formulation for inkjet printing of optoelectronics and photonics *Nat. Commun.* **8** 278
[16] Lotya M *et al* 2009 Liquid phase production of graphene by exfoliation of graphite in surfactant/water solutions *J. Am. Chem. Soc.* **131** 3611–20
[17] Secor E B, Prabhumirashi P L, Puntambekar K, Geier M L and Hersam M C 2013 Inkjet printing of high conductivity, flexible graphene patterns *J. Phys. Chem. Lett.* **4** 1347–51
[18] Gao Y, Shi W, Wang W, Leng Y and Zhao Y 2014 Inkjet printing patterns of highly conductive pristine graphene on flexible substrates *Ind. Eng. Chem. Res.* **53** 16777–84
[19] Kelly A G *et al* 2017 All-printed thin-film transistors from networks of liquid-exfoliated nanosheets *Science* **356** 69–73
[20] Cunningham G, Hanlon D, McEvoy N, Duesberg G S and Coleman J N 2015 Large variations in both dark-and photoconductivity in nanosheet networks as nanomaterial is varied from MoS_2 to WTe_2 *Nanoscale* **7** 198–208
[21] Zhao Y *et al* 2017 Doping, contact and interface engineering of two-dimensional layered transition metal dichalcogenides transistors *Adv. Funct. Mater.* **27** 1603484
[22] Esmaeili-Rad M R and Salahuddin S 2013 High performance molybdenum disulfide amorphous silicon heterojunction photodetector *Sci. Rep.* **3** 2345
[23] Ghanbarzadeh S, Abbaszadeh S and Karim K S 2014 Low dark current amorphous silicon metal–semiconductor–metal photodetector for digital imaging applications *IEEE Electron Device Lett.* **35** 235–7
[24] Ha D, Fang Z and Zhitenev N B 2018 Paper in electronic and optoelectronic devices *Adv. Electron. Mater.* **4** 1700593
[25] T Vicente A *et al* 2018 Multifunctional cellulose-paper for light harvesting and smart sensing applications *J. Mater. Chem.* C **6** 3143–81
[26] Aga R S, Lombardi J P, Bartsch C M and Heckman E M 2014 Performance of a printed photodetector on a paper substrate *IEEE Photonics Technol. Lett.* **26** 305–8
[27] Zhou Y and Reed E J 2015 Structural phase stability control of monolayer $MoTe_2$ with adsorbed atoms and molecules *J. Phys. Chem.* C **119** 21674–80
[28] Keum D H *et al* 2015 Bandgap opening in few-layered monoclinic $MoTe_2$ *Nat. Phys.* **11** 482–6
[29] Li Y, Duerloo K A N, Wauson K and Reed E J 2016 Structural semiconductor-to-semimetal phase transition in two-dimensional materials induced by electrostatic gating *Nat. Commun.* **7** 1–8
[30] Song S *et al* 2016 Room temperature semiconductor-metal transition of $MoTe_2$ thin films engineered by strain *Nano Lett.* **16** 188–93

[31] Riaz A et al 2015 Light emission, light detection and strain sensing with nanocrystalline graphene *Nanotechnology* **26** 325202
[32] Castellanos-Gomez A, Quereda J, van der Meulen H P, Agraït N and Rubio-Bollinger G 2016 Spatially resolved optical absorption spectroscopy of single- and few-layer MoS_2 by hyperspectral imaging *Nanotechnology* **27** 115705
[33] Cunningham G et al 2012 Percolation scaling in composites of exfoliated MoS_2 filled with nanotubes and graphene *Nanoscale* **4** 6260–4
[34] Wang Q H, Kalantar-Zadeh K, Kis A, Coleman J N and Strano M S 2012 Electronics and optoelectronics of two-dimensional transition metal dichalcogenides *Nat. Nanotechnol.* **7** 699–712
[35] Lanzillo N A, Simbeck A J and Nayak S K 2015 Strain engineering the work function in monolayer metal dichalcogenides *J. Phys.: Condens. Matter* **27** 175501
[36] Britnell L et al 2013 Strong light–matter interactions in heterostructures of atomically thin films *Science* **340** 1311–4